Spot-Scan Imaging in Transmission Electron Microscopy

KENNETH H. DOWNING

The determination of the structure of proteins and other organic materials by transmission electron microscopy is a rapidly developing field. Obtaining high-resolution images of these radiation-sensitive specimens has, until recently, been problematic. The development of spot-scan imaging, in which the electron beam is focused to a spot with a diameter of about 1000 angstroms and moved over the specimen to record the image, has overcome some of the most severe problems, which result from beam-induced motion of the specimen and its image. Elimination of this motion greatly enhances the contrast of high-resolution features of the image and promises a significant increase in the speed with which future structural work can be accomplished.

ELECTRON MICROSCOPY HOLDS GREAT PROMISE AS A TOOL in the determination of molecular structures. Electron crystallography (*1*) in particular represents a newly developed method that should allow the solution of the structure of complex molecules at atomic resolution in those previously intractable cases where the available crystals are too thin and small to use for x-ray crystallography. The ability to obtain information at high resolution is a prerequisite for success. Electron diffraction data can be obtained quite easily to well beyond 3 Å resolution for a number of protein and other organic specimens. If one could also obtain lattice images to about 3.5 Å resolution, from which structure factor phases could then be determined (*2*), standard crystallographic refinement procedures could be used to determine the structure to the resolution limit of the electron diffraction data. Although the difficulty of obtaining high-quality image data is, in practice, greater than the difficulty of collecting good diffraction patterns, the structure of one membrane protein, bacteriorhodopsin, has recently been obtained to high enough resolution to allow a chain-tracing model to be built (*3*), and rapid progress on a number of other protein structures can now be expected.

Many factors can conspire to make imaging more difficult than obtaining diffraction patterns, mainly by decreasing the contrast at high resolution. Henderson and Glaeser (*4*) have reviewed these factors and their relative effects on the image. The electron microscope itself is not one of the main factors. Instrumental resolution has been available well beyond 3.5 Å for several generations of microscopes, although the limited spatial and temporal coherence of the illumination do cause some reduction in high-resolution contrast. Instead, most of the limiting factors are ultimately a result of the radiation sensitivity of organic specimens. The essential problem of high-resolution imaging lies in obtaining as much information as possible before the specimen becomes too severely damaged by the imaging process itself.

The one factor that most affects image quality often proves to be beam-induced specimen motion, which may cause a loss of about a factor of 5 in image contrast at a resolution near 4 Å in specimens that are sensitive to beam damage (*4*). Several forces will tend to make a specimen move in several different modes under electron beam irradiation. Breakage of covalent bonds necessarily increases interatomic distances from values characteristic of covalent bonds to those characteristic of van der Waals contacts. The force that this expansion can generate within the specimen is sufficient to distort any organic specimen (*5*). Countering this force, mass loss from volatilization of small radiolytic fragments may make specimens shrink or collapse. Other effects, namely, specimen charging and heating, will, under some conditions, also cause image degradation through movement of the specimen or image.

Henderson and Glaeser suggested a logical approach to reducing the amount and effects of beam-induced motion. If the area of the specimen that is illuminated at a given time were reduced, the stress resulting from structural changes (as well as from charging and heating) would also be reduced and the surrounding, unirradiated area would restrain the specimen against any residual stress. The small illumination spot can be deflected across the specimen, moving either continuously or in discrete steps, to expose the photographic film. Such images are now called "spot-scan" images. Efficient spot-scan imaging systems have been implemented in my laboratory (*6, 7*) and by Bullough and Henderson (*8*) to test this hypothesis.

With these systems beam-induced motion effects can be reduced, if not virtually eliminated, and there is a significant improvement in image quality. In this article, the implementation of such systems is reviewed along with some of the recent results obtained in my laboratory with a variety of specimens.

Spot-Scan Imaging

A stringent requirement for the implementation of a spot-scan system is that a small beam spot must be formed and the coherence required for good phase-contrast imaging must be retained. So that spatial coherence does not limit the image resolution, one must ensure that the angle subtended by the source from the specimen is less than about 0.1 mrad (*9*). At an accelerating voltage of 100 keV, the diffraction-limited spot size is about 400 Å with this beam angle.

If the electron source is imaged onto the specimen at condenser crossover, a second condenser aperture with a diameter less than about 40 μm is necessary to keep the illumination angle below 0.1 mrad. With a conventional (tungsten hairpin) illumination system,

The author is in the Donner Laboratory, Lawrence Berkeley Laboratory, University of California, Berkeley, CA 94720.

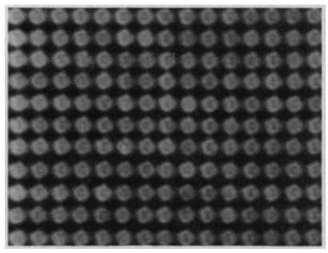

Fig. 1. Spot-scan image. Images are typically recorded by stepping the beam through a raster of 15 by 11 points filling the area of a photographic film. In this case, the magnification is 56,000 and the spot diameter and spacing are about 1000 Å. Each spot is a highly defocused image of the condenser aperture; the non-uniform intensity within each spot arises from Fresnel fringes around its edge. A small, 60-Hz interference produces further effects similar to moire fringes.

it is also necessary to highly excite the first condenser lens in order to produce a small enough spot. It would be difficult with a conventional electron gun to obtain enough brightness to allow short exposure times on each spot. In our implementation, a field emission source is used that produces about 1000 times the brightness of a conventional source. This system allows operation with moderate first-condenser excitation, and a second-condenser aperture about 20 μm in diameter.

A lanthanum hexaboride (LaB_6) source, which provides a brightness about ten times that of a conventional system, should also meet the requirements for beam size and intensity. This type of gun was used by Bullough and Henderson (*8*) and by researchers at several other laboratories where spot-scan systems have been implemented. Since the brightness of an electron gun scales with accelerating voltage, operation at voltages above 100 keV will also aid in producing a small, bright spot.

It is convenient to overfocus the condenser to give a slightly larger illuminated spot, improving the coherence and, in our system, minimizing the effect of a 60-Hz field interference that deflects the beam up to several hundred angstroms. The crossover point is set about 1 mm above the specimen, so that each point on the specimen is illuminated by a 400 Å diameter source that subtends a half-angle of about 2×10^{-5} rad.

The beam position can be controlled during a scan in several different ways. Many of the basic requirements are met in the current generation of microscopes, which contain microprocessors for digital control of operation. Computer control of beam position has been added through analog interfaces to the electronics of our JEM 100B electron microscope. This is perhaps an inelegant approach, but it is particularly straightforward in this case and has been effective. The computer can also control both condenser lenses, the objective focus, and intermediate lens (for diffraction focus) to allow convenient switching between operations such as searching for good specimen areas, focusing, and recording an image or diffraction pattern.

Reducing the beam diameter to about 1000 Å appears to eliminate most beam-induced motion under many circumstances. Several situations are mentioned below where it may be desirable to use an even smaller beam. The beam is stepped over the specimen in a raster that is generally between 10 by 15 and 20 by 30 spots, exposing a full film at ×50 to ×60,000 magnification (Fig. 1). The exposure time is typically 0.03 to 0.1 s per spot, with a beam intensity set to give a total exposure of 5 to 15 electrons per square angstrom (e/Å^2) to the specimen. The total exposure time of about 15 s may stretch the limits of stability of older high-voltage and lens current supplies, but even longer exposure times could be used with newer, more stable instruments.

Experimental Results

Paraffin. The most extensive quantitative work documenting the benefits of the spot-scan technique (*6–8*) has been done with monolamellar crystals of paraffin. Paraffin was chosen as a test specimen for several reasons. Its primary lattice spacings are about 4 Å, in the range where a significant improvement in image contrast is needed. The susceptibility of paraffin to radiation damage, as judged by the fading of electron diffraction patterns with accumulated exposure, is quite similar to that of most protein crystals that have been studied. In addition, it is easy to obtain crystals of paraffin that are of a defined, uniform thickness, which makes quantitative analysis of image contrast straightforward. Interpretation of some of the results of these experiments was aided by knowledge of the radiation chemistry of paraffin (*10*). One disadvantage of using paraffin as a model specimen, however, is that mass loss is virtually nonexistent in comparison to that in proteins and some other polymers.

The small unit cell of paraffin, as with other small organic molecules, concentrates the scattered electron intensity into fewer diffraction spots than with most protein crystals. This makes the image contrast so high that it is fairly easy to resolve the 4 Å lattice lines even when image contrast is severely degraded by beam-induced motion. Indeed, lattice images of paraffin have been recorded with conventional, flood illumination by a number of groups. Zemlin and co-workers (*11*) obtained good results and resolution to 2.5 Å with the superconducting-lens microscope in Berlin. However, the quantitative measurements of Henderson and Glaeser (*4*) indicated that in the best images the image contrast was only about 3% of what it would have been in an ideal image, with beam-induced motion apparently accounting for the loss of a factor of 5 in contrast.

Paraffin crystals that are to be imaged are carefully selected for

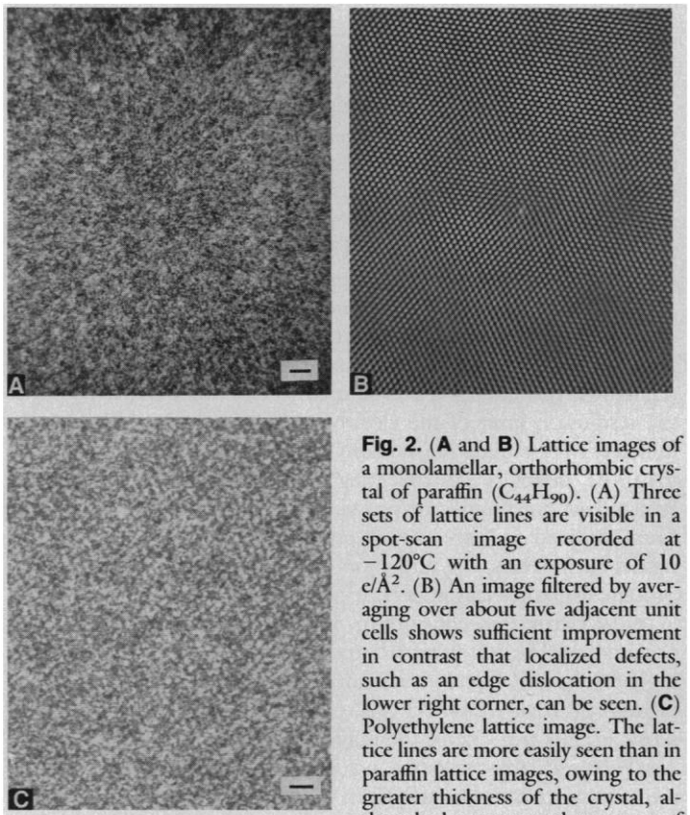

Fig. 2. (**A** and **B**) Lattice images of a monolamellar, orthorhombic crystal of paraffin ($C_{44}H_{90}$). (A) Three sets of lattice lines are visible in a spot-scan image recorded at −120°C with an exposure of 10 e/Å^2. (B) An image filtered by averaging over about five adjacent unit cells shows sufficient improvement in contrast that localized defects, such as an edge dislocation in the lower right corner, can be seen. (**C**) Polyethylene lattice image. The lattice lines are more easily seen than in paraffin lattice images, owing to the greater thickness of the crystal, although the corrugated structure of the crystal makes it hard to find areas where all three principal lattice lines have good contrast. The greater thickness also makes the crystal more subject to beam-induced motion, which tends to reduce the contrast in the direction of local movement. This image was recorded with a relatively low exposure at 3 e/Å^2. Scale bars = 10 Å.

isotropic diffraction so that all three of the primary lattice lines should show about the same contrast. Even so, in nearly all of the conventional images the contrast in at least one direction was worse than in the other two directions. Different areas on a single micrograph often showed best contrast in different directions. This effect is interpreted as evidence for differential motion of the specimen under illumination, with different areas moving in different directions.

In the small-spot images of paraffin, the diffraction spots from the images, observed on an optical diffractometer, are significantly brighter than for images produced with flood illumination, and most of the images show isotropic contrast. Quantitative measurement of image contrast confirms that the contrast in spot-scan images is higher, typically by a factor of 3 to 5 (*6*).

The fraction of good-quality images is far greater with small-spot illumination than with flood illumination. Bullough, for example, found about an eightfold improvement in the number of images that were judged by several criteria to be good (*12*). His measurements also point out that the degree of improvement increases with the total specimen exposure; at very low exposure there is little motion and little to be gained with the spot-scan system. At higher doses to the specimen, which improve the signal-to-noise (*S/N*) ratio in the image and increase the amount of information obtained, the improvement of spot-scan over conventional imaging increases. In the case of paraffin, it is even possible to raise the *S/N* ratio enough to be able to see the lattice directly on the electron microscope (EM) negative, with no image enhancement. A section of one image is shown where all three of the principal lattice lines are visible (Fig. 2A).

This image is still quite noisy, given the limited exposure to the specimen. The Rose equation can be used to estimate how much exposure and contrast are required to visualize an image such as this by relating the minimum size or spacing d of an object with contrast C that can be resolved when imaged with n quanta (electrons) per unit area:

$$d = a/C\sqrt{n}$$

The factor a, usually taken as 5 for isolated objects, is close to 1 for sets of parallel lines (*13*). At an exposure of 10 e/Å^2 and with a measured contrast in this image of 0.12, the 4 Å lattice should be just visible. The structure of isolated features, such as point defects in the lattice, however, would not be visible in such an image. The visibility of the lattice, and to some extent of defects, can be improved if the image is filtered (Fig. 2B). The filter in this image corresponds to averaging over an area with a diameter of about five unit cells, and, although it reveals the lattice lines with excellent contrast, it tends to spread out the image of isolated features in the lattice. Defects such as an edge dislocation in the lower right corner, however, are still well resolved.

The factor of 3 to 5 improvement in image contrast implies that beam-induced motion can be virtually eliminated. These images of paraffin are good in most respects, but they consistently show one defect (*7*). The contrast for each set of lattice lines is best in a band running through the center of the exposed spot, parallel to the lines. Thus, different areas of the image within the small illumination spots show good contrast for the different orientations of the lattice. This effect can be interpreted as a result of the particular radiation

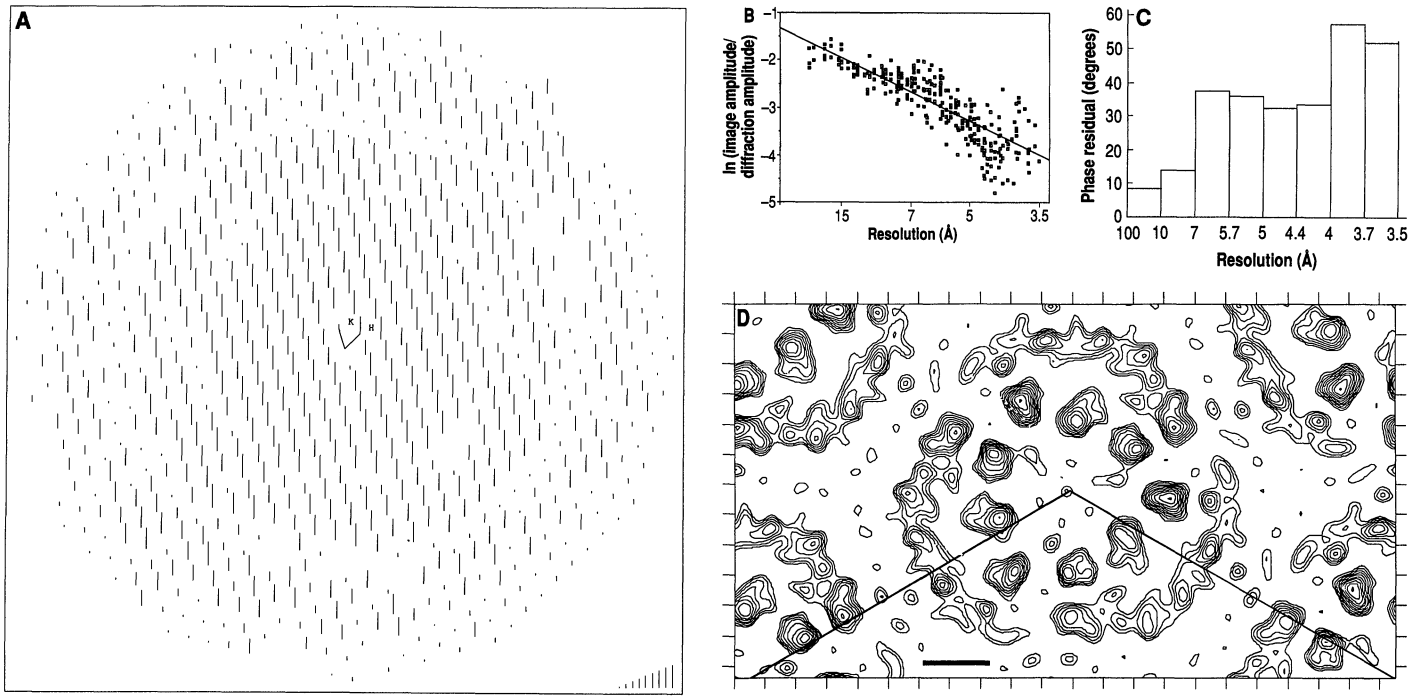

Fig. 3. (**A**) Diffraction spots found in the Fourier transform of a spot-scan image of PM. The image was recorded with an exposure of 6 e/Å^2, and an area corresponding to 1 μm^2 on the specimen was digitized in a 6000 by 6000 array for computer processing. The length of line segments at each reciprocal lattice point indicates the peak-to-background ratio for measured diffraction spots; length is proportional to 10-IQ, with IQ defined in (*16*). The nine segment lengths used are shown in the lower right corner. The edge of the plot corresponds to a resolution of 3.5 Å. There is a high density of good data out to at least 3.5 Å. Zeros of the contrast transfer function appear as rings where only weak spots are detected. (**B**) Falloff of image contrast with increasing resolution. The ratio of the diffraction amplitude from the Fourier transform of a spot-scan image to the corresponding electron diffraction amplitude, plotted as the natural logarithm, decreases with increasing resolution at a rate that is about one-third as fast as previously seen (*16*), and slightly slower than in the previous best images (*17*). (**C**) The differences between structure factor phases obtained from one spot-scan image of PM and those in (*16*), which were obtained by combining 12 images, are plotted in resolution zones. These differences are comparable to the internal consistency of the previous data. (**D**) The projection map of bR calculated from data in three spot-scan images (top) shows essentially all features in the map (bottom) that was calculated from combined data from 12 images (*16*). Scale bar = 10 Å.

chemistry of paraffin. There is relatively little mass loss from paraffin as it undergoes radiation damage; rather, some hydrogen is lost, with accompanying accumulation of double bonds. This results in shortening and thickening of the paraffin chains, which in turn causes an increase in the projected area of the molecules. Thus, within each small illuminated area there is a radial expansion during the recording of the image, which causes loss of contrast near the edge of the area except where the lattice lines run parallel to the radial expansion. Evidence of this expansion can be seen in the surface relief of specimens that are heavy metal–shadowed after exposure to the beam (7). Fortunately, this effect appears to occur only with paraffin.

Polyethylene. The structure of crystalline polyethylene is quite similar to that of paraffin, with extended chains running through the narrow dimension of the plate like crystals and with the same bond lengths and angles (*14*). The polyethylene chains, much longer than paraffin, are not fully extended but fold back and forth in the crystal, producing a thickness of about 120 Å. A difference of particular importance in this work is that the solution-grown polyethylene crystals collapse when applied to an EM grid from a pyramidal form to a highly corrugated structure. Because polyethylene crystals are more than twice as thick as paraffin, it is not difficult to obtain lattice images of polyethylene in which the lattice lines are visible. Indeed, Revol and Manley (*15*) obtained such images even at room temperature, without the use of spot-scan imaging. However, the stress associated with the corrugations appears to lead to the dominant mode of beam-induced specimen motion, namely, large-scale motions that cause reorientation of the crystals. The greater thickness also increases the effect of small specimen tilts on the image. This motion is easily seen in the movement of bend contours in the image, and it severely limits the electron exposure that can be used in recording reliable images. The difference between conventional and spot-scan images of polyethylene is at least as great as with paraffin, particularly when higher exposures are used. Both the frequency with which good images are obtained and the contrast within the images are markedly improved. An example of the type of improved lattice image contrast that can be obtained with the spot-scan mode is shown in Fig. 2C.

Purple membrane. Purple membrane (PM), isolated from the bacterium *Halobacterium halobium*, contains one protein, bacteriorhodopsin (bR), in a naturally crystalline array. Much of electron crystallography has developed around this specimen, with the purposes of understanding the protein's structure-function relation and of using PM to test various imaging and image processing schemes. In this work, PM has served as a good test specimen, allowing quantitative comparison of results from conventional and spot-scan imaging. This work has been carried out as part of the ongoing structure determination of bR in an attempt to obtain images of higher quality than is generally possible with conventional techniques.

Two reports on high-resolution studies of PM (*16, 17*) serve as reference for much of this analysis. In one (*16*), 12 images recorded with conventional illumination on three different microscopes were combined to produce a 3.5 Å projection map, with an estimated figure of merit of 0.8 and phase error below 30° in the resolution range of 5 to 3.5 Å. Subsequently, a set of images obtained with the superconducting-lens microscope in Berlin was used to extend the resolution in the map to 2.8 Å.

The analysis of several spot-scan images (Fig. 3, A and B) can be compared to similar published results. The diffraction peaks that were found in the computed Fourier transform of one spot-scan image are shown in Fig. 3A. Line segments are drawn at the locations of each reciprocal lattice point, with the length indicating the strength of the peak at that point. The zeros of the contrast transfer function (CTF) are clearly evident out to high resolution. The number of spots detected in the transform of this image (314) is significantly greater than in any of the images in (*16*) (maximum of 256), but less than the number in the images in (*17*) (up to 377). Some variation in the number of spots arises from the defocus value of the image, the area of the micrograph that is processed, and the exact treatment used in image processing.

The rate of falloff of the diffraction peak amplitudes with increasing resolution may be a better measure of quality. The ratio of peak amplitudes in the image transform to the amplitudes determined from electron diffraction is plotted as a function of resolution in Fig. 3B. In a perfect image, the points would lie on a line with a slope of zero. In (*16*), the ratio decreases at a rate corresponding to a loss of a factor of 30 in contrast at 4 Å. In (*17*), the factors that gave improved images resulted in a falloff of only a factor of 15. In Fig. 3B, the falloff amounts to a factor of only 10.

This rate of falloff can be accounted for almost entirely by instrumental effects and the modulation transfer function of the photographic film, indicating that, as with paraffin, images can be obtained in which beam-induced motion does not occur. In contrast

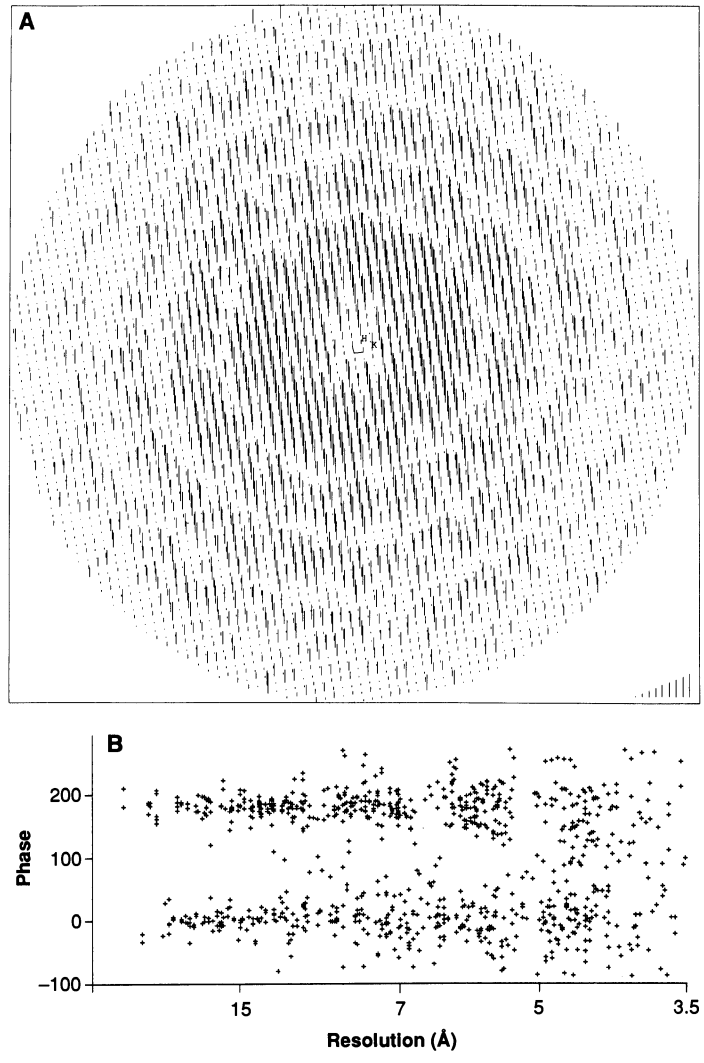

Fig. 4. (**A**) Plot of diffraction spots found in the computed Fourier transform of an image of PhoE porin shows over 1200 peaks, with a peak-to-background ratio of at least 1. With the high density of reciprocal lattice points, which arises from the large unit cell, the CTF zeros are particularly evident. (**B**) Phases from one spot-scan image of PhoE porin, after phase origin refinement and correction for beam tilt, agree quite well with the symmetry-constrained values of 0° or 180° out to high resolution.

to the experience with paraffin, no changes in surface relief could be detected with PM, even with high electron exposure (*18*), confirming that there is no net force to expand the crystal with increasing radiation damage.

A further measure of the quality that can be obtained from a spot-scan image is given by considering the phase error in this image with respect to the phases determined in (*16*). A plot of this phase difference as a function of resolution is shown in Fig. 3C. The phase difference between this single image and combined data from the 12 previous images is comparable, particularly at high resolution, to the difference between two halves of the previous data [figure 8 in (*16*)]. This result confirms that we can obtain about the same quality of data from a single spot-scan image as from the average of several conventional images.

A real-space view of the image quality is given in Fig. 3D, which shows a PM projection calculated from data in three spot-scan images, along with part of the image presented in (*16*). In this case it is necessary to combine data from more than one image to fill in the zeros in the transfer function as much as to build up an adequate *S/N* ratio. The agreement in details is quite striking. In particular, the features resolved simultaneously in both of these independent images can be taken to represent real details of the protein structure.

PhoE porin. PhoE porin, one of the pore-forming proteins from the outer membrane of *Escherichia coli*, has been reconstituted into crystalline membrane sheets that diffract to well beyond 3 Å (*19*). The large unit cell of these crystals, 150 Å by 130 Å, decreases diffraction amplitudes and makes it more difficult to obtain high-resolution image data than with PM. Even so, high-quality images have been obtained with the small-spot illumination. The spots with good *S/N* ratio detected in the transform of one image are shown in Fig. 4A. Significantly more spots were detected in the transform of the best spot-scan images (1260) than in the best flood-beam images (850). In this case, the quality of the images can be judged by the agreement of the phases with either 0° or 180°, as constrained by the *pgg* symmetry of the projection. A plot of the image phases determined from this image is shown in Fig. 4B, corrected for phase origin and beam tilt. The average phase error from 0° or 180° is below 20° to 5 Å, and 30° from 5 to 3.5 Å. A projection map with resolution of about 3.5 Å has been calculated from the combined data of eight images and shows a number of significant features of the β-sheet structure that forms the channel (*20*).

Light-harvesting complex. The light-harvesting complex, a membrane-bound protein occurring in chloroplasts of most green plants, has been reconstituted into monolayer, crystalline sheets and studied by electron crystallography (*21*). As with PhoE porin, a large unit cell combined in this case with a low density of protein within the unit cell produces rather weak diffraction and low image contrast. However, excellent images were obtained with the spot-scan technique that allowed reconstruction of a 3.7 Å projection map (*21*).

The high degree of symmetry provides a measure of the quality of the image data. A projection calculated from data contained in a single spot-scan image is shown in Fig. 5A. Although no symmetry has been imposed in this image, the two trimers within the unit cell, one oriented up and the other down in the crystal, appear as mirror images. In addition, the threefold symmetry within each trimer is strong in all details. It is thus apparent that from a single image data of high quality can readily be obtained, even with rather difficult specimens. Upon averaging data from three images, the phase error was only 30° in the 5 to 3.5 Å range, indicating that the map is reliable.

Tobacco mosaic virus (TMV). In some recent work, good images of TMV have been obtained and analyzed in conjunction with the previously determined x-ray structure to produce a map with about 9 Å resolution (*22*). These images were obtained with the specimen

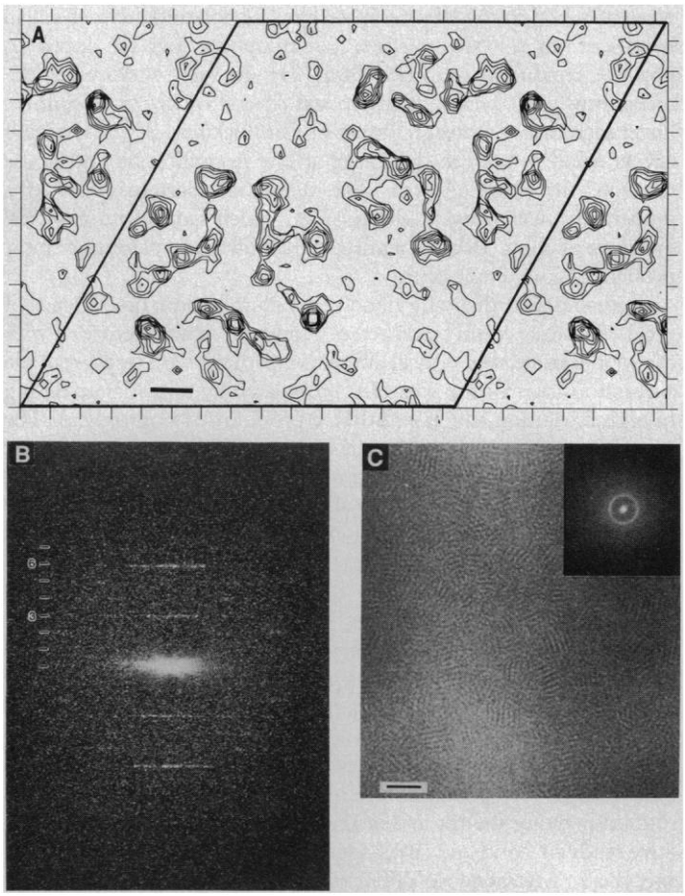

Fig. 5. (**A**) Projection map of light-harvesting complex obtained from a single spot-scan image. No symmetry has been imposed in this image, but the p321 symmetry of the crystal is apparent in high-resolution details. Scale bar = 10 Å. (**B**) Optical transform of a spot-scan image of glucose-embedded TMV shows strong contrast out to at least the sixth layer line, corresponding to a resolution better than 10 Å. Layer line numbers are marked on the left. This image was recorded at ×56,000 magnification with an exposure of 12 e/Å². (**C**) A spot-scan image of polythiophene shows good high-resolution detail, including a mosaic of domains with 17 Å spacing, in spite of very low conductivity of the sample. **Inset**: an optical transform of the image. Scale bar = 100 Å.

embedded in a thin layer of vitreous ice. Some attempts were made in my laboratory to image TMV embedded in a film of glucose suspended over holes in a holey film. Specimens embedded in both vitreous ice and glucose suffer from the potential problem that the embedding medium has much less electrical conductivity than a carbon film. Thus, specimen charging could present a serious problem, the effects of which would be similar to beam-induced motion. In addition, glucose of this thickness is highly susceptible to bubbling under electron irradiation, leading to particularly bizarre beam-induced motion.

Images of different areas of the glucose-embedded TMV were recorded with small-spot and flood-beam illumination. Although the flood-beam images consistently showed virtually no optical diffraction from the TMV, the small-spot images showed optical diffraction of very good quality. An optical diffraction pattern from one of these images (Fig. 5B) compares quite favorably with a corresponding pattern from the average of several ice-embedded specimens (*22*). Note in particular that diffraction is seen on all layer lines out to at least the sixth, with the intensity on the sixth even higher than that on the third layer line, as it is in x-ray diffraction patterns from ordered aggregates of TMV (*23*).

Polythiophene. In the course of some thin-film studies, images

were obtained in my laboratory of films of polythiophene that had been cast on a water surface. Polythiophene can be doped to produce conductive polymer films (*24*). In these undoped specimens, however, the conductivity was several orders of magnitude lower than that of a carbon film of similar thickness. Severe charging effects could be seen in the image at low magnification and in the electron diffraction pattern. The diffraction patterns showed a moderately sharp ring at about 17 Å, which faded with a critical exposure of about 10 e/Å^2, similar to the diffraction patterns of most proteins at low temperature.

In images recorded with flood beam illumination, no evidence of the 17 Å lattice could be detected. However, images recorded with the spot-scan showed optical diffraction patterns with rings from the amorphous part of the specimen modulated by the CTF extending to high resolution and in addition, a pronounced ring at 17 Å. The 17 Å lattice could be seen directly on the image in small domains of about 100 Å diameter. One such image and its optical transform are shown in Fig. 5C. This result shows that with low-conductivity specimens, specimen charging problems can be significantly reduced if the illuminated area is reduced, and high-resolution images can be obtained.

Bizarre phenomena with tilted specimens. When imaging tilted specimens, one may observe that the resolution in the direction perpendicular to the tilt axis is significantly worse than that in the direction parallel to the axis. This effect is attributable to vibration of the specimen in a drumhead motion perpendicular to the plane of the specimen. In particularly severe cases, the effect can cause a limitation to very poor resolution in one direction, even when the resolution along the tilt axis is apparently unaffected. In a comparative study of flood and small-spot illumination on images of tilted specimens, a tremendous difference was observed in the resolution given by the two methods in the direction perpendicular to the axis.

Optical transforms of two images taken from adjacent areas of the same large PM patch, which had been tilted by 30°, are shown in Fig. 6. Flood illumination yielded resolution hardly better than 50 Å perpendicular to the tilt axis (Fig. 6A), while the spot-scan image (Fig. 6B) shows much better resolution in this direction. The extent of the resolution loss is particularly great in this case, and the example shown therefore dramatizes how great the improvement from small-spot illumination can be, even in the worst cases. More importantly the side-by-side comparison of the difference between flood illumination and spot-scan images illustrates that the loss is apparently related to electron irradiation rather than to vibrational resonance. It is not clear whether this effect is primarily due to radiation damage or specimen charging. On this particular EM grid, nearly all of the flood-beam images showed comparably poor resolution, with the small-spot images much better in each comparative pair, independent of which of a pair was recorded first.

Although this motion is generally far less severe than in this example, it may account for much of the difficulty encountered in obtaining images of tilted PM specimens that show isotropically good resolution (*3*). Further reduction of spot size and beam current may reduce the effect even further.

Other Considerations for Spot-Scan Imaging

Exposure time. The brightness of the field emission source is high enough to give a current density in the small spot that is at least an order of magnitude higher than normally used for flood beam illumination, resulting in an exposure time per small spot about one-tenth of that used for conventional images. Drift problems, which often limit the performance of the microscope, are thus reduced by a factor of 10 and have not been a significant problem in recent work. However, the total exposure time for recording an entire image is about ten times as long, increasing the demands on stability of the high voltage and of the lens current if one requires the image focus to remain constant. If the focus does change by more than an acceptable amount during a long exposure, one could always treat each small-spot image separately, rather than process a whole field of spots as a single image. There are other reasons why one might want to handle the data in this way, and thus some attention has been given to the optimal method of combining small areas of statistically noisy images (*25*).

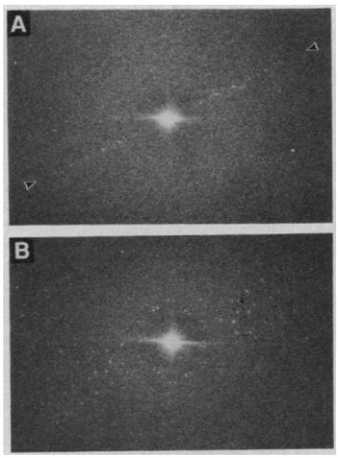

Fig. 6. Comparison of (**A**) flood-beam and (**B**) spot-scan images of a PM specimen tilted to 30°. This area includes two crystals with different orientations. Optical transforms show good resolution in both images along the tilt axis (arrowheads). Resolution perpendicular to the axis is severely limited by apparent motion of the flood-beam image, and is greatly improved in the spot-scan image. Decrease of diffraction spot intensities away from the tilt axis are characteristic of specimens with imperfect flatness (see text).

Data collection by video system. For many years, electron microscopists have envisioned collection of image data by video pickup systems. Particularly in the case of crystallographic studies, this approach has seemed impractical because the large image fields and the large number of image elements that are required for obtaining a high *S/N* ratio are far greater than in a video image. The ability to treat small-spot images individually makes it appealing to consider video systems again, because for each small-spot image the number of image elements is compatible with available video systems. In particular, the image could be stepped across a video camera in synchrony with the beam stepping (so that the beam remains stationary on the camera). Image areas could be treated separately as described above or brought into register with each other in the image-processing computer for treatment as a single large field.

Correction for defocus ramp. A natural enhancement of spot-scan images of tilted specimens involves on-line correction for the defocus ramp across the specimen area being imaged. In a conventional image, the defocus across the tilted specimen can vary so greatly that only a small region of the film is close enough to focus to give optimal contrast. In the case of a spot-scan image, one can orient the scan lines parallel to the tilt axis, and reset the objective lens focus for each scan line to keep the entire image at essentially the same focus. Zemlin (*26*) has already demonstrated the principle of this type of dynamic focus correction, albeit in a somewhat different context. An example of the effect of this correction is shown in Fig. 7. In an image of a specimen tilted at 45° without focus compensation, defocus goes from overfocus at one edge to underfocus at the other, where the CTF oscillates quite rapidly. With the focus compensation switched on, the image stays in focus across the whole field.

There will still be a defocus gradient across each of the small-spot areas. One can treat this gradient, as well as any residual defocus gradient over the whole image that is not compensated by the electronics, as described in (*3*) by defining the contrast pattern for each Fourier component over the image area. Although this will be a more complex pattern than the sinusoidal pattern that occurs in the case of a conventional image, multiplying the image by the contrast

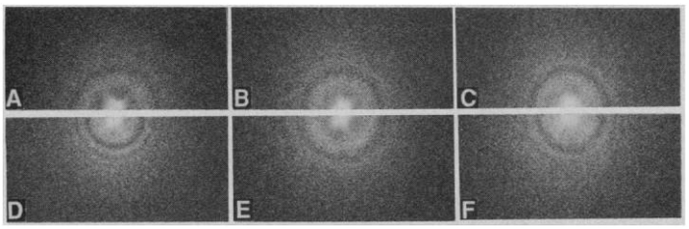

Fig. 7. Dynamic focus correction in spot-scan images. Two spot-scan images of the same specimen tilted at 45° were recorded, with the focus correction switched on in (**A**, **B**, and **C**), and off in (**D**, **E**, and **F**). Optical transforms from the same areas of the two micrographs are shown (A and D, area at top of micrograph; B and E, middle; C and F, bottom).

pattern still compensates for the defocus gradient as before. The benefit of dynamic adjustment is that the defocus value can be kept within a range such that the spatial coherence envelope function (*9*) does not take too severe a toll on the signal (contrast) at high resolution.

In this context, the use of higher accelerating voltage should be advantageous in reducing the defocus change across the small spot. The shorter electron wavelength should allow formation of a smaller spot and, at the same time, increase the depth of field.

Conclusion

In high-resolution imaging of specimens that are sensitive to damage or charging, spot-scan illumination can provide an important improvement over conventional illumination. This finding has been confirmed in several laboratories where spot-scan methods have been implemented with a wide variety of organic specimens. Although the best conventional images may be of the same high quality as the spot-scan images, the conventional yield of very good images has been painfully low. In other cases, spot-scan images provide resolution that is unattainable with conventional illumination. Much of our work in electron crystallography and other high-resolution studies has been limited by the low *S/N* ratio in the image. The ability that spot-scan imaging provides to obtain images reliably and routinely with nearly the theoretically full *S/N* ratio represents a major advance in the ease with which structural studies can now proceed.

REFERENCES AND NOTES

1. R. M. Glaeser, *Annu. Rev. Phys. Chem.* **36**, 243 (1985).
2. W. Hoppe, *Acta Crystallogr. Sect. A* **26**, 414 (1970).
3. R. Henderson *et al.*, *J. Mol. Biol.* **213**, 899 (1990).
4. R. Henderson and R. M. Glaeser, *Ultramicroscopy* **16**, 139 (1985).
5. J. M. McBride, B. E. Segmuller, M. D. Hollingsworth, D. E. Mills, B. A. Weber, *Science* **234**, 830 (1986).
6. K. H. Downing and R. M. Glaeser, *Ultramicroscopy* **20**, 269 (1986).
7. K. H. Downing, *ibid.* **24**, 387 (1988).
8. P. Bullough and R. Henderson, *ibid.* **21**, 223 (1987).
9. J. Frank, *Optik (Stuttgart)* **38**, 519 (1977).
10. H. Orth and E. W. Fischer, *Makromol. Chem.* **88**, 118 (1965).
11. F. Zemlin, E. Reuber, B. Beckmann, E. Zeitler, D. L. Dorset, *Science* **229**, 461 (1985).
12. P. Bullough, *Electron Microsc. Rev.* **3**, 249 (1990).
13. A. Rose, *Vision: Human and Electronic* (Plenum, New York, 1973), p. 18.
14. C. W. Bunn, *Trans. Faraday Soc.* **35**, 482 (1939).
15. J.-F. Revol and R. St. John Manley, *J. Mater. Sci. Lett.* **5**, 249 (1986).
16. R. Henderson, J. M. Baldwin, K. H. Downing, J. Lepault, F. Zemlin, *Ultramicroscopy* **19**, 147 (1986).
17. J. M. Baldwin, R. Henderson, E. Beckmann, F. Zemlin, *J. Mol. Biol.* **202**, 585 (1988).
18. K. H. Downing, unpublished results.
19. B. K. Jap, *J. Mol. Biol.* **205**, 407 (1989).
20. ——, K. H. Downing, P. Walian, *J. Struct. Biol.* **103**, 57 (1990).
21. W. Kuhlbrandt and K. H. Downing, *J. Mol. Biol.* **207**, 823 (1989).
22. T.-W. Jeng, R. A. Crowther, G. Stubbs, W. Chiu, *ibid.* **205**, 251 (1989).
23. K. C. Holmes, G. J. Stubbs, E. Mandelkow, U. Gallwitz, *Nature* **254**, 192 (1975).
24. O. A. Patil, A. J. Heeger, F. Wudl, *Chem. Rev.* **88**, 183 (1988).
25. D. R. Brillinger, K. H. Downing, R. M. Glaeser, G. A. Perkins, *J. Appl. Stat.* **16**, 165 (1989).
26. F. Zemlin, *J. Electron. Microsc. Tech.* **11**, 251 (1989).
27. This work was supported in part by the Office of Health and Environmental Research, U.S. Department of Energy, under contract DE-AC03-76SF00098 and by NIH research grant PO1-GM36884. Polyethylene specimens were kindly provided by D. Vesely, PhoE porin by B. Jap, light-harvesting complex by W. Kuhlbrandt, TMV by D. L. D. Caspar, and polythiophene by A. J. Heeger.